Acta Crystallographica Section A
Foundations of Crystallography
ISSN 0108-7673

Received 14 March 2005
Accepted 3 June 2005

Refinement of the crystal structural parameters of $La_{2/3}Ca_{1/3}MnO_3$ using quantitative convergent-beam electron diffraction

Fang Feng, Jing Zhu* and Aihua Zhang

Electron Microscopy Laboratory, School of Materials Science and Engineering, Tsinghua University, Beijing 100084, People's Republic of China. Correspondence e-mail: jzhu@mail.tsinghua.edu.cn

Crystal structural parameters (seven positional parameters and four isotropic Debye–Waller factors) of $La_{2/3}Ca_{1/3}MnO_3$ have been refined using the quantitative convergent-beam electron diffraction (QCBED) method. Using intensity information of many higher-order Laue-zone reflections simultaneously is essential to refine structural parameters accurately. The effective global optimization algorithm was used to avoid the problems of input values and local minima. The fittings of the differential coefficients of one-dimensional experimental intensities and theoretical ones calculated by the dynamical diffraction theory were carried out with the normalized Euclidean distance criterion. Thus, all of these improve the accuracy and reliability of the analysis. The calculated results with the refined parameters agree with the experiments. The refined parameters also agree with the Rietveld refinement results of neutron diffraction.

1. Introduction

In recent years, determinations of crystal structural parameters using the quantitative convergent-beam electron diffraction (QCBED) method have been attempted. Vincent *et al*. (1984*a*,*b*) first applied the QCBED method under the quasi-kinematical approximation to determine atomic positions. Zuo & Spence (1991) first introduced an automatic program into the QCBED method to refine structure parameters. The method was used to determine the structure parameters of metals and intermetallics by many groups (such as Holmestad *et al*., 1993; Rossouw *et al*., 1996; Midgley *et al*., 1996; Nüchter *et al*., 1998; Saunders *et al*., 1999*a*,*b*; Wu, Li *et al*., 2000; Wu, Zhu *et al*., 2000). Jansen *et al*. (1998) determined atomic positions of $La_3NiB_2N_3$, $ThPd_{0.65}B_{4.7}$ and $Ce_5Cu_{19}P_{12}$. Now the challenge is to use the QCBED method to determine the structure parameters of perovskite-like materials. Some attempts and results have been reported (Tsuda & Tanaka, 1995, 1999; Tsuda *et al*., 2002; Feng *et al*., 2004; Ogata *et al*., 2004). The process of the QCBED method is to fit the theoretical reflection intensity distribution to the experimental zero-dimensional (integrated intensities), one-dimensional (line profiles) or two-dimensional intensities of zeroth-order Laue-zone (ZOLZ) and higher-order Laue-zone (HOLZ) reflections. More details of the concepts and theory of the QCBED method can be seen in the book by Spence & Zuo (1992).

The QCBED method based on the dynamical diffraction theory has the following advantages compared to X-ray and neutron diffraction methods. (i) the QCBED method enables one to determine the structure, from specimen areas of a few nanometres in diameter, of not only perfect crystals but also imperfect parts of crystals. (ii) Structure factors of low-order reflections in electron diffraction are more sensitive to the distributions of valence electrons. (iii) CBED intensities contain stronger phase information of structure factors through the dynamical diffraction effect. (iv) It is possible to obtain comprehensive information by combining QCBED with other techniques, such as high-resolution imaging, composition analysis and electron energy-loss spectrum analysis, in a transmission electron microscope (TEM) (Zhu *et al*., 1998).

Colossal magnetoresistance (CMR) has been found in $La_{2/3}Ca_{1/3}MnO_3$ (Jin *et al*., 1994). Although the mechanism of CMR is not very clear yet, the phase-separation phenomenon on the micro- or nanometre scale and the Jahn–Teller effect are closely related to CMR (Radaelli *et al*., 1995; Ramirez *et al*., 1996; Dagotto *et al*., 1998; Hennion *et al*., 1998). It is difficult with X-ray and neutron diffraction techniques to obtain diffraction intensity data from such a small single domain but this is easy with the convergent-beam electron diffraction (CBED) technique.

In this work, experimental data pre-processing and the analysis software were improved. The seven atomic positional parameters and four isotropic Debye–Waller factors of $La_{2/3}Ca_{1/3}MnO_3$ were refined using one-dimensional intensity profiles of HOLZ discs in three CBED patterns by using the QCBED method.

2. Experiment and calculation

Our QCBED method (Feng *et al.*, 2004) is based on fitting the differential coefficient of the one-dimensional experimental intensity profile of a CBED pattern to a theoretical one calculated by the dynamical diffraction theory. The flowchart in Fig. 1 demonstrates the procedure of the QCBED method. Some important items of the analysis procedure are discussed below.

2.1. Experiment

The sample was synthesized by the solid-state reaction method at 1623 K in air for 48 h and was annealed at 1163 K in N_2 for 12 h. The nominal composition is $La_{2/3}Ca_{1/3}MnO_3$. The thin-foil specimen for the CBED experiment was prepared by ion milling.

A JEM-2010F TEM equipped with TVIPS TemCam-F114 slow-scan charge-coupled device (CCD) camera was used to obtain digital CBED patterns. The TEM was operated at an accelerating voltage of 200 kV. A liquid-nitrogen trap was used to eliminate the radiation damage and contaminations in the column.

We took three CBED patterns with incidences near the [201] zone axis. Enough reflections were excited simultaneously along this direction while too many reflections were excited in the case of the lower zone-axis pattern. The patterns were taken with a probe of about 1 nm in diameter from three different points of the same region. The diffraction patterns of $La_{2/3}Ca_{1/3}MnO_3$ were indexed under the space group *Pnma*, in which lattice parameters of the unit cell were set as a = 5.451, b = 7.700 and c = 5.467 Å as reported by Kaduk & Wong-Ng (1997). The values of Debye–Waller factors, $B_{La} = B_{Ca} = 0.38$, $B_{Mn} = 0.21$, $B_{O(1)} = 0.47$ and $B_{O(2)} = 0.53$ Å^2 for lanthanum calcium manganese oxide at 150 K, taken from the literature (Dai *et al.*, 1996), were used as medians of their initial value ranges in fittings. The atomic coordinate set of $La_{2/3}Ca_{1/3}MnO_3$ and the ranges of their initial values are listed in Table 1, where δ is the radius of the ranges. The experimental line profiles of HOLZ reflections were acquired along the radial direction.

Table 1
Atomic sites of the *Pnma* phase of $La_{2/3}Ca_{1/3}MnO_3$.

Element	Wyckoff position	Coordinate	Range of initial values
La/Ca	4*c*	*x*, 1/4, *z*	0.02±δ, 1/4, 0±δ
Mn	4*b*	0, 0, 1/2	0, 0, 1/2
O(1)	4*c*	*x*, 1/4, *z*	0.49±δ, 1/4, 0.06±δ
O(2)	8*d*	*x*, *y*, *z*	−0.275±δ, −0.033±δ, 0.275±δ

2.2. Distortion correction of CBED patterns

The use of HOLZ reflections is essential because those reflections with large reciprocal vectors are sensitive to small displacements of atoms and Debye–Waller factors. However, the distortion of CBED patterns caused by lens aberration and the relative orientation between the CCD and the optical axis of the TEM can be omitted for ZOLZ reflections but it is appreciable when considering the HOLZ reflections. It is necessary to correct the distortion of a CBED pattern before using its HOLZ intensities for an accurate fitting.

The procedure is similar to that described by Tsuda *et al.* (2002). The distortion due to lenses is assumed to be proportional to the cube of the distance from the optical axis. The distortion due to the relative orientation is elliptical. An example of the distortion correction is shown in Fig. 2. The real positions of the HOLZ reflection discs (the dark lines) without and with distortion correction are shown in Figs. 2(*a*) and 2(*b*), respectively. It is seen that the experimental HOLZ reflections agree much better with the positions of the circles in Fig. 2(*b*).

Small residual displacements of CBED patterns still exist even after correction of the pattern distortion as above. Some geometrical parameters can be introduced in the fittings to adjust further the positions and lengths of the one-dimensional profiles of the reflection discs. These are two positional

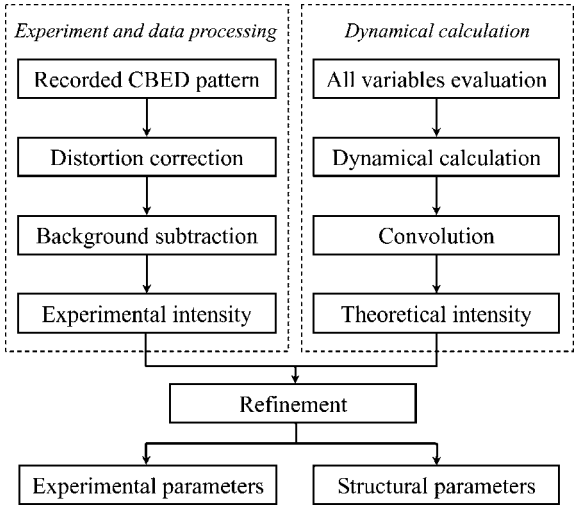

Figure 1
Flowchart of the procedure of the QCBED method.

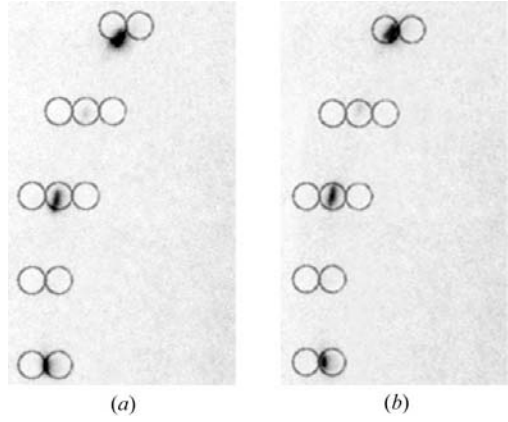

Figure 2
Correction of the distortion due to the lens aberrations and the detective device CCD. HOLZ reflection discs are shown from one CBED pattern of $La_{2/3}Ca_{1/3}MnO_3$ in negative contrast (*a*) without and (*b*) with the distortion correction, respectively. The positions of the HOLZ reflections calculated by the lattice parameters are indicated by black circles.

parameters for the starting point of each profile line, one parameter for its length, and one angle parameter for its orientation. But in the present work, only a few geometrical parameters of the intensity profile lines were adjusted in the fittings. Most geometrical parameters were kept unchanged in order to test whether the whole procedure is robust and feasible. Further, one should be very cautious when deciding whether to adjust one geometrical parameter or not.

2.3. Background subtraction

The application of the method without an energy filter requires very thin specimens for reducing inelastic background intensity and suppressing the intensity variation of HOLZ reflections along the azimuthal direction due to dynamical diffraction (Tsuda & Tanaka, 1995).

However, the weak background still needs special consideration. The background intensity in each reflection disc was subtracted by linear interpolation between the background intensities just outside the disc. It works well for the areas with a monotonic background. We did not use such reflection discs where more than two Kikuchi lines or bands intersect. Furthermore, the effect of the background intensity is also considered in the fitting process (see §2.5 for details).

2.4. Dynamical calculation

The intensity calculation is based on the Bloch-wave formulation of dynamical theory, namely matrix diagonalization of many-beam equations (Hirsch, 1977; Spence & Zuo, 1992). Crystal potentials used for the many-beam equation were calculated using electron atomic scattering factors of Doyle & Turner (1968), atomic positions, Debye–Waller factors and site occupancies. Symmetrically equivalent atomic positions were generated automatically using space-group symmetries. We have employed the imaginary potential given by the subroutine *ATOM* (Bird & King, 1990) as the default absorption potential to describe absorption due to inelastic scattering. To obtain accurate intensities of HOLZ reflections, the absorption potential was treated by solving the complex matrix of the dynamical theory.

The convergence of the dynamical theory calculation relies on the number of reflections involved in the calculation. The reflections used in the scattering matrix were selected by the method of Zuo & Weickenmeier (1995) and Birkeland *et al.* (1996). $g_{\max}$, $s_{g\max}$, $B_{\min}$, $s_{gs\max}$ and $\omega_{\max}$ are five beam-selection criteria. $g_{\max}$ is the maximum length of g and those reflections beyond this range are not considered at all. Then, the reflection is selected when $|2Ks_g|$ is less than $s_{g\max}$, where s_g is the excitation error and K is the wavevector of the reflection. The perturbation strength criterion ($|U_g/2Ks_g| > B_{\min}$) was used as a supplementary selection criterion because even reflections with structure factor $U_g \approx 0$ are often important through dynamical interaction. All selected reflection beams are divided into two groups, either so-called 'strong beams' or 'weak beams'. If $|2Ks_g|$ is less than $s_{gs\max}$ or $|Ks_g/U_g|$ is less than $\omega_{\max}$, the reflection is regarded as a strong beam. The effects of weak beams were incorporated into the crystal-potential coefficients of strong beams in the Bethe-potential method in order to reduce the order of the initial matrix to be diagonalized.

We have assumed a Gaussian function as the instrumental function and have convoluted the Gaussian function into the calculated intensities.

2.5. Global optimization program

Atomic positions, Debye–Waller factors, specimen thickness, incidence direction and geometrical parameters were refined simultaneously in the fitting. We have developed a global optimization program with the effective global optimization algorithm (Stougie, 1982) for such calculations to avoid the local minimum problem. In our program, a unique manner to calculate the goodness of fit (GOF) was adopted. It arises from the consideration of the background that cannot be removed thoroughly by energy filter and background subtraction. This kind of background can be assumed as constant within a small range, such as in one CBED HOLZ disc. The unknown constant background is implicitly eliminated by fitting the calculated derivatives of the intensity with respect to the position coordinate, $I^{\mathrm{theo}'}(i)$, to the corresponding experimental values, $I^{\mathrm{exp}'}(i)$, where i labels the pixel along the line profile. The fitting is done with the normalized Euclidean distance (NED) criterion (Hofmann & Ernst, 1994) in our program. The NED criterion that is supposed to descend smoothly (Li *et al.*, 2000) is more suitable for most optimization algorithms.

$$\mathrm{NED}(I^{\mathrm{exp}'}, I^{\mathrm{theo}'}) = \left\{ \frac{\sum_i [I^{\mathrm{exp}'}(i) - I^{\mathrm{theo}'}(i)]^2}{\{\sum_i [I^{\mathrm{exp}'}(i)]^2 \sum_i [I^{\mathrm{theo}'}(i)]^2\}^{1/2}} \right\}^{1/2}.$$

3. Results

Fig. 3 shows the three CBED patterns of $La_{2/3}Ca_{1/3}MnO_3$. ZOLZ reflections are seen at the center of the patterns and first-order Laue-zone (FOLZ) reflections as rings in the outer part. The percentage ratio of background intensities outside the reflection discs to the intensity maxima inside them was less than 30% for the ZOLZ reflections and approximately 10% for the FOLZ reflections.

Two independent sets of one-dimensional intensities of the same 48 FOLZ reflections of each pattern were extracted after distortion correction and background subtraction. Six sets of intensity data were obtained from the three independent CBED patterns. For each set of intensities, one independent refinement of the same parameters was performed with the global optimization program. The total number of data points used for each fitting was 720 from a certain CBED pattern and 15 points in each of the 48 line profiles.

As described in the previous paper by Feng *et al.* (2004), the incidence direction was determined by two coordinates of the zone-axis center projected onto the CBED pattern. The possible range of zone-axis center of each CBED pattern was estimated approximately within a square region, shown by the

white square in Fig. 3(*a*). The initial values of specimen thicknesses were set within the range of 100 to 1500 Å. The incident-beam direction and thickness were refined in the first step. The specimen thickness was determined to be around 400 Å by comparing experimental ZOLZ CBED patterns with calculated ones while the approximate incident-beam direction was obtained. In the next step, the search ranges of thickness and incident direction were narrowed by the above results and positional parameters were added to be refined. The initial values of atomic positions were set in the ranges as listed in Table 1, with $\delta = 0.01$. The results of the second step were used to narrow the search space further. In the final step, all the parameters including the isotropic Debye–Waller factors were refined. To shorten the computing time, the global refinements were performed in three steps.

From the results of the convergence tests of intensities with the number of reflections, about 512 reflections were taken for the dynamical calculations of the [201] pattern with the parameters $g_{\max} = 4.0$ Å^{-1}, $s_{g\ \max} = 1.0$ Å^{-1}, $s_{gs\max} = 0.3$ Å^{-1}, $B_{\min} = 0.01$ and $\omega_{\max} = 5.0$. About 370 reflections were treated as weak beams by the Bethe-potential method.

The fitting result for one data set is shown in Fig. 4 as an example. The one-dimensional intensities of 48 reflections with indices given below are shown in the graphs. Most of the calculated intensities are seen to agree well with the experimental ones. Most reflections are fitted accurately enough that the final NED value of the fitting is 0.38. The profile fitting of some reflections is not so good and these show a shift of the experimental *versus* theoretical position of the intensity maximum. This is partially because of an insufficient adjustment of the geometrical parameters.

From the six independent fittings, the seven positional parameters and four Debye–Waller factors were determined. The refined structure parameters, which are the average values of the independent fittings, are listed in the second column of Table 2. The values in parentheses are the standard uncertainties (s.u.'s) of the refined parameters derived from the six independent fittings. Generally, the s.u.'s of the fractional coordinates of lanthanum and calcium are smaller than those of oxygen, and those of the O(1) atoms at the apex position of the MnO_6 octahedron are much larger than the others. The s.u.'s of the oxygen Debye–Waller factors are larger than those of lanthanum and manganese.

Fig. 5 shows the refined crystal structure of $La_{2/3}Ca_{1/3}MnO_3$. The distortion of the octahedron is clearly seen in the structure. The bond lengths and angles were calculated from the refined positional parameters and the lattice parameters reported by Kaduk & Wong-Ng (1997) with an assumption

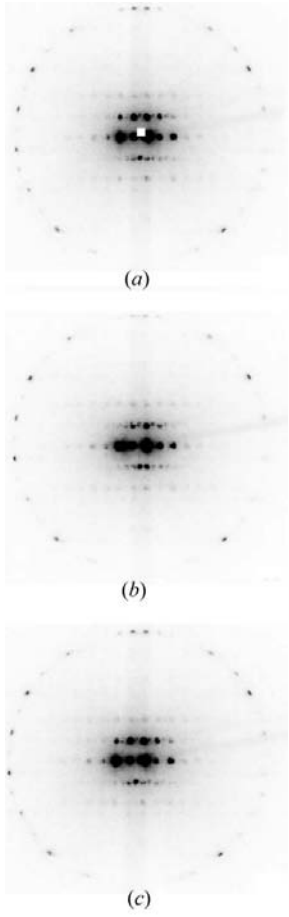

Figure 3
CBED patterns of $La_{2/3}Ca_{1/3}MnO_3$ taken near the [201] zone axis.

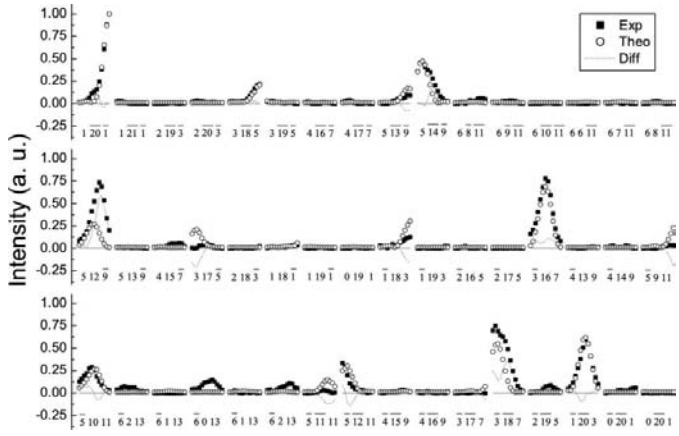

Figure 4
Intensity comparison for one fitting result. The experiment and theoretical calculations are indicated by solid squares and hollow circles, respectively. The difference between them is shown by the dashed line.

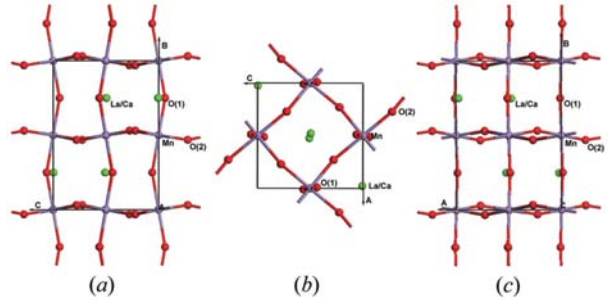

Figure 5
The refined structure of $La_{2/3}Ca_{1/3}MnO_3$.

Table 2
Positional parameters and Debye–Waller factors of $La_{1-x}Ca_xMnO_3$.

	QCBED	Neutron diffraction					
Ca doping	0.33	0.30	0.30	0.33	0.33	0.34	0.375
T (K)		270	300	270	298	275	300
a (Å)	5.451	5.46558 (3)	5.46597 (4)	5.4575 (1)	5.4569 (1)	5.464 (2)	5.4730 (5)
b (Å)	7.700	7.72035 (4)	7.72603 (6)	7.7126 (2)	7.7112 (1)	7.716 (2)	7.7309 (9)
c (Å)	5.467	5.48494 (4)	5.48237 (5)	5.4728 (2)	5.4717 (1)	5.473 (2)	5.4875 (1)
La/Ca							
x	0.0232 (16)	0.0185 (6)	0.0197 (3)	0.0212 (3)	0.0187 (1)	0.024 (1)	0.0209 (7)
z	−0.006 (2)	−0.007 (1)	−0.0050 (5)	−0.0049 (5)	−0.0035 (2)	−0.009 (2)	−0.0044 (7)
B (Å^2)	0.386 (12)	0.27 (5)	0.38 (1)	0.68 (2)	−0.11 (1)	0.9	0.71 (4)
Mn							
B (Å^2)	0.212 (6)	0.24 (6)	0.22 (2)	0.56 (3)	−0.11 (1)	0.9	0.69 (1)
O(1)							
x	0.489 (11)	0.490 (1)	0.4913 (5)	0.4910 (5)	0.4916 (8)	0.488 (1)	0.4948 (4)
z	0.061 (17)	0.0608 (9)	0.0637 (5)	0.0631 (4)	0.0588 (14)	0.062 (2)	0.0637 (1)
B (Å^2)	0.47 (3)	0.51 (7)	0.62 (3)	0.82 (3)	−0.11 (1)	1.3	0.72 (4)
O(2)							
x	−0.271 (2)	−0.2759 (6)	−0.2751 (3)	−0.2766 (3)	−0.2786 (11)	−0.275 (2)	−0.2761 (2)
y	−0.031 (4)	−0.0344 (4)	−0.0330 (2)	−0.0330 (2)	−0.0333 (3)	−0.032 (1)	−0.0315 (1)
z	0.2767 (10)	0.2761 (6)	0.2755 (3)	0.2771 (3)	0.2781 (11)	0.277 (2)	0.2762 (8)
B (Å^2)	0.54 (3)	0.54 (5)	0.63 (2)	0.94 (3)	−0.11 (1)	1.6	0.89 (9)

The refined results of the QCBED method are given in the second column. Several results of neutron Rietveld analysis from the literature are listed in the right-hand columns for comparison. The third and fourth column results were reported by Hibble *et al.* (1999), the fifth column by Huang *et al.* (1998), the sixth column with an average Debye–Waller factor B = −0.11 (1) Å^2 by Blasco *et al.* (1996), the seventh column by Simopoulos *et al.* (1999) and the last column by Yang *et al.* (2004).

that the lattice parameters in the small specimen region were the same. The bond length of Mn—O(1) along the b axis of the unit cell is 1.95 (2) Å while the bond lengths of Mn—O(2) in the plane of the MnO_6 octahedron split into two values, one shorter 1.931 (5) and one longer 1.976 (5) Å. The bond angle of Mn—O(1)—Mn along the b axis is 160 (1)°. Those of Mn—O(2)—Mn in the plane are 162.2 (3)°. Details of interatomic distances and bond angles are shown in Table 3.

Table 3
Selected interatomic distances (Å) and angles (°) for $La_{2/3}Ca_{1/3}MnO_3$.

	QCBED	Neutron diffraction analysis		
Doping	0.33	0.33	0.33	0.33
T (K)		270	300	298
La/Ca—O(1)	2.93 (2)	2.920 (3)	2.915 (2)	
La/Ca—O(1)	2.57 (2)	2.592 (3)	2.596 (2)	
La/Ca—O(1)	3.04 (2)	3.056 (4)	3.061 (3)	
La/Ca—O(1)	2.44 (2)	2.423 (4)	2.426 (3)	
La/Ca—O(2) ×2	2.62 (1)	2.636 (2)	2.639 (2)	
La/Ca—O(2) ×2	2.74 (1)	2.751 (2)	2.754 (2)	
La/Ca—O(2) ×2	3.11 (1)	3.134 (2)	3.127 (1)	
La/Ca—O(2) ×2	2.48 (1)	2.446 (2)	2.454 (2)	
Mn—O(1) ×2	1.95 (2)	1.9601 (4)	1.961 (3)	1.955 (1)
Mn—O(2) ×2	1.931 (5)	1.958 (2)	1.958 (1)	1.959 (6)
Mn—O(2) ×2	1.976 (5)	1.964 (2)	1.966 (1)	1.963 (6)
Mn—O(1)—Mn ×2	160 (1)	159.4 (1)	159.7 (1)	160.9 (3)
Mn—O(2)—Mn ×4	162.2 (3)	160.56 (9)	160.75 (6)	160.4 (14)

Some selected interatomic distances and bond angles determined by the refined results of the QCBED method are given in the second column. Neutron Rietveld analysis results of Huang *et al.* (1998) are also listed in the third and fourth columns and those of Blasco *et al.* (1996) are listed in the last column for comparison.

4. Discussion

4.1. Line profile of CBED pattern

It is necessary to include a large number of reflections in the calculations to ensure convergence of the solution of the dynamical diffraction theory for QCBED. Furthermore, a large amount of data with some extent of redundancy is useful to improve the accuracy and reliability of the refinement.

However, limited computing capacity in contrast to the increase of both the reflections in the dynamical theoretical calculation and the variables in the fittings means that a balance is needed between accuracy and performance efficiency. The redundancy of data in one-dimensional profiles is much lower than that in two-dimensional intensities. The computation can be carried out on a common PC or workstation. For example, one dual-CPU workstation, which is configured with two PIII-800M Xeon CPUs, 512 Mbyte ECC memory, and a 18 Gbyte SCSI hard disk and Linux operating system with kernel version 2.4.7–10, was used in our study to perform the fittings. About 10^5 s and more than 200 calculations of the object function are needed on average to determine one local minimum in the final step.

Relatively fertile information is contained in line profiles. Fitting of a one-dimensional intensity profile is more economical in time than that of two-dimensional intensities while it is more accurate than that of integrated intensities (zero dimensional). It is the most important reason that line profiles were used in the multiparameter refinement.

In addition, there are other advantages in using a one-dimensional profile. For instance, it is easy to use derivatives of intensities instead of intensities in the fitting so as to reduce further the effect of the residual background.

4.2. Evaluation of experimental error

Standard uncertainties of crystal structural parameters are usually evaluated by the error-propagation rule. However, the s.u.'s from the error-propagation rule are underestimated probably because of the correlations between data points in CBED patterns (Ogata *et al*., 2004). Furthermore, operations, such as determining the position/direction and re-sampling the experimental pattern, can also introduce errors that are difficult to include using the error-propagation rule. In the present study, we carried out six independent fittings of the 11 structure parameters for three similar CBED patterns. The s.u.'s of these parameters were estimated as the standard deviations of their averages.

The values in parentheses following the interatomic distances and angles were calculated by the error-propagation rule according to the relation between them and the atomic position parameters regardless of the errors of the lattice parameters. In this case, the errors would be underestimated.

4.3. Convergence and reliability

The convergence of the refinement is accompanied by an increase in reflections included in the calculation (Zuo & Weickenmeier, 1995). The convergence of the fits with changes of reflection number was examined by the method of Zuo & Weickenmeier (1995). More than 300 reflections were needed in the fits and the reflections belonging to the second-order Laue zone with g up to 4.0 Å^{-1} were included.

In our global optimization algorithm, the input values of all parameters to be refined and their range are just used to define a parameter search space. Every point in the parameter search space represents a set of initial values for a local search. The choice of a particular point depends on whether it is unclustered or clustered in the global algorithm. Also, local minima are not restricted within the search space. So our fitting results are not associated rigorously with the values that are input into the program.

Some results of similar doping levels obtained by neutron diffraction analysis in the literature (Blasco *et al*., 1996; Huang *et al*., 1998; Hibble *et al*., 1999; Simopoulos *et al*., 1999; Yang *et al*., 2004) are also shown in Table 2 for comparison. It is seen that the values of the different neutron Rietveld analyses vary greatly around the most interesting calcium doping level (x = 0.33). Our electron diffraction results agree with these values, especially with those of $La_{0.70}Ca_{0.30}MnO_3$ (listed in the third and fourth columns in Table 2) in spite of some discrepancies in the x coordinates of La and O(2) and the Debye–Waller factor B_{La}. There may be two main reasons for the discrepancies in structural parameters. One probable reason is that the temperature of the experiment is near the Curie temperature of a magnetic (metal–insulator) transition. It is reported that structure readjustment of $La_{2/3}Ca_{1/3}MnO_3$ is pronounced at the transition from insulating to metallic behavior and is associated with anomalously high values of the atomic thermal parameters in a range of temperatures around the Curie temperature (Dai *et al*., 1996; Huang *et al*., 1998). Another possible reason is changes of composition, for example, the inhomogeneity reported to occur with a phase-separation phenomenon in this material (Fath *et al*., 1999; Milward *et al*., 2005). The results of the QCBED method were obtained from a very local area in the specimen while the results of neutron diffraction are the average information of crystals. The result of energy-dispersive X-ray spectroscopy analysis also shows composition inhomogeneity with a few Ca-rich regions in the specimen (the results will be published elsewhere). The loss of calcium during the synthesis and annealing process is also probable. Either the metal–insulator transition or the phase-separation phenomenon is closely related to the CMR effect. The discrepancies may contain useful information.

Thus, the present method can provide reasonable structural parameters for such materials. Independence from the input value also raises the possibility of analysis of more complex materials or local structures of imperfect crystals.

5. Concluding remarks

We have applied the QCBED method to the structure analysis of $La_{2/3}Ca_{1/3}MnO_3$, for which 11 structure parameters were refined. The MnO_6 octahedra are distorted. The bond lengths of manganese and oxygen in the plane of the MnO_6 octahedron split to a shorter one and a longer one. The calculated intensities are seen to agree with the experimental intensities and the structure parameters agree with some results of neutron Rietveld analysis.

The use of one-dimensional CBED intensities of many HOLZ reflections simultaneously enables accurate fitting of structural parameters and thus ensures the accuracy and reliability of the analysis. The fitting was carried out with little dependence of the global optimization algorithm on the input values. The good convergence of dynamic theoretical calculations and the reliability of the results make the QCBED method possible for more applications.

We would like to express our gratitude to Professor J. M. Zuo, Professor Y. G. Zhao and Dr M. Y. Wu for helpful discussions and suggestions. This work is financially supported by National 973 Project of China, Chinese National Nature Science Foundation and National Center for Nanoscience and Technology of China.

References

Bird, D. M. & King, Q. A. (1990). *Acta Cryst.* A**46**, 202–208.
Birkeland, C., Holmestad, R., Marthinsen, K. & Hoier, R. (1996). *Ultramicroscopy*, **66**, 89–99.
Blasco, J., Garcia, J., de Teresa, J. M., Ibarra, M. R., Algarabel, P. A. & Marquina, C. (1996). *J. Phys. Condens. Matter*, **8**, 7427–7442.
Dagotto, E., Yunoki, S., Malvezzi, A. L., Moreo, A., Hu, J., Capponi, S., Poilblanc, D. & Furukawa, N. (1998). *Phys. Rev. B*, **58**, 6414–6427.
Dai, P., Zhang, J. D., Mook, H. A., Foong, F., Liou, S. H., Dowben, P. A. & Plummer, E. W. (1996). *Solid State Commun.* **100**, 865–869.
Doyle, P. A. & Turner, P. S. (1968). *Acta Cryst.* A**24**, 390–397.

Fath, M., Freisem, S., Menovsky, A. A., Tomioka, Y., Aarts, J. & Mydosh, J. A. (1999). *Science*, **285**, 1540–1542.
Feng, F., Zhang, A. H. & Zhu, J. (2004). *Ultramicroscopy*, **98**, 173–185.
Hennion, M., Moussa, F., Biotteau, G., Rodriguez-Carvajal, J., Pinsard, L. & Revcolevschi, A. (1998). *Phys. Rev. Lett.* **81**, 1957–1960.
Hibble, S. J., Cooper, S. P., Hannon, A. C., Fawcett, I. D. & Greenblatt, M. (1999). *J. Phys. Condens. Matter*, **11**, 9221–9238.
Hirsch, P. B. (1977). *Electron Microscopy of Thin Crystals.* Malabar, FL: R. E. Krieger Publishing Co.
Hofmann, D. & Ernst, F. (1994). *Ultramicroscopy*, **53**, 205–221.
Holmestad, R., Weickenmeier, A. L., Zuo, J. M., Spence, J. C. H. & Horita, Z. (1993). *Electron Microsc. Anal.* **138**, 141–144.
Huang, Q., Santoro, A., Lynn, J. W., Erwin, R. W., Borchers, J. A., Peng, J. L., Ghosh, K. & Greene, R. L. (1998). *Phys. Rev. B*, **58**, 2684–2691.
Jansen, J., Tang, D., Zandbergen, H. W. & Schenk, H. (1998). *Acta Cryst.* A**54**, 91–101.
Jin, S.,Tiefel, T. H., Mccormack, M., Fastnacht, R. A., Ramesh, R. & Chen, L. H. (1994). *Science*, **264**, 413–415.
Kaduk, J. & Wong-Ng, W. (1997). ICDD Grant-in Aid, NIST, Ceramics Division, Gaithersburg, MD, USA.
Li, S. Y., Wu, M. Y. & Zhu, J. (2000). *Ultramicroscopy*, **83**, 103–109.
Midgley, P. A., Sleight, M. E. & Vincent, R. (1996). *J. Solid State Chem.* **124**, 132–142.
Milward, G. C., Calderon, M. J. & Littlewood, P. B. (2005). *Nature (London)*, **433**, 607–610.
Nüchter, W., Weickenmeier, A. L. & Mayer, J. (1998). *Acta Cryst.* A**54**, 147–157.
Ogata, Y., Tsuda, K., Akishige, Y. & Tanaka, M. (2004). *Acta Cryst.* A**60**, 525–531.
Radaelli, P. G., Cox, D. E., Marezio, M., Cheong, S. W., Schiffer, P. E. & Ramirez, A. P. (1995). *Phys. Rev. Lett.* **75**, 4488–4491.
Ramirez, A. P., Schiffer, P., Cheong, S. W., Chen, C. H., Bao, W., Palstra, T. T. M., Gammel, P. L., Bishop, D. J. & Zegarski, B. (1996). *Phys. Rev. Lett.* **76**, 3188–3191.
Rossouw, C. J., Gibson, M. A. & Forwood, C. T. (1996). *Ultramicroscopy*, **66**, 193–209.
Saunders, M., Fox, A. G. & Midgley, P. A. (1999*a*). *Acta Cryst.* A**55**, 471–479.
Saunders, M., Fox, A. G. & Midgley, P. A. (1999*b*). *Acta Cryst.* A**55**, 480–488.
Simopoulos, A., Pissas, M., Kallias, G., Devlin, E., Moutis, N., Panagiotopoulos, I., Niarchos, D., Christides, C. & Sonntag, R. (1999). *Phys. Rev. B*, **59**, 1263–1271.
Spence, J. C. H. & Zuo, J. M. (1992). *Electron Microdiffraction.* New York: Plenum Press.
Stougie, L. (1982). *Math. Program.* **22**, 125.
Tsuda, K., Ogata, Y., Takagi, K., Hashimoto, T. & Tanaka, M. (2002). *Acta Cryst.* A**58**, 514–525.
Tsuda, K. & Tanaka, M. (1995). *Acta Cryst.* A**51**, 7–19.
Tsuda, K. & Tanaka, M. (1999). *Acta Cryst.* A**55**, 939–954.
Vincent, R., Bird, D. M. & Steeds, J. W. (1984*a*). *Philos. Mag.* A**50**, 745–763.
Vincent, G., Bird, D. M. & Steeds, J. W. (1984*b*). *Philos. Mag.* A**50**, 765–786.
Wu, M. Y., Li, S. Y., Zhu, J., Du, Z. H. & Li, S. L. (2000). *Acta Cryst.* A**56**, 189–192.
Wu, M. Y., Zhu, J., Li, S. Y., Du, Z. H. & Li, S. L. (2000). *J. Appl. Cryst.* **33**, 1119–1121.
Yang, C. H., Song, J. H., Park, S. H., Choi, Y. N., Lee, C. H. & Jeong, Y. H. (2004). *J. Phys. Soc. Jpn*, **73**, 3051–3058.
Zhu, J., Duan, X. F., Li, D. X. & Ye, H. Q. (1998). *Microsc. Res. Tech.* **40**, 122–135.
Zuo, J. M. & Spence, J. C. H. (1991). *Ultramicroscopy*, **35**, 185–196.
Zuo, J. M. & Weickenmeier, A. L. (1995). *Ultramicroscopy*, **57**, 375–383.